Technical Note

Landslides (2023) 20:1705–1718
DOI 10.1007/s10346-023-02062-2
Received: 6 December 2022
Accepted: 19 March 2023
Published online: 26 April 2023

Jan Lenart · Martin Kašing · Tomáš Pánek · Régis Braucher · František Kuda

Rare, slow but impressive: > 43 ka of rockslide in river canyon incising crystalline rocks of the eastern Bohemian Massif

Abstract Despite significant progress in understanding the stability of rock slopes, little is known about the time scales of the evolution of slow-moving rockslides. The Ledové sluje rockslide in the Thaya River canyon is a unique and infrequent slope failure developed in crystalline rocks of the Variscan orogen in Central Europe. Fresh topography with trenches, rock walls, slided blocks, scree slopes and crevice-type caves has attracted generations of geologists for more than a century, but questions of mechanism and age of the rockslide have remained unresolved. To address this question, we combined geomorphological research with detailed analysis of the geological structure, electrical resistivity profiling and terrestrial cosmogenic nuclide dating (TCN). Our data show that failure developed above the river undercut bank along a planar sliding surface predisposed by NW-oriented gently dipping metamorphic foliation intersected by steep fractures and faults. Although TCN dating does not allow determination of the entire life span of the rockslide, its scarp predisposed by NE- to ENE-striking fault was largely exposed in the Last Glacial during marine isotope stages (MIS) 3 and 2 between ~ 43 and 23 ka, suggesting slow gradual or multievent movement of the rockslide slope rather than a single catastrophic event. We conclude that, although very rare in Central Europe, rockslides in the crystalline rocks of the Palaeozoic orogens may leave a much longer topographic footprint than in the adjacent Alpine mountain belts.

Keywords Crevice-type cave · Electrical resistivity tomography · Orthogneiss · Structural analysis · Terrestrial cosmogenic nuclide dating

Introduction

Rockslides developed in crystalline rocks are commonly described from world mountain belts such as the European Alps (Strauhal et al. 2017; Zangerl et al. 2010), Carpathians (Němčok 1972; Pánek et al. 2016, 2017) and High Asia (Schramm et al. 1998; Weidinger and Korup 2009), but they are less common in pre-Cenozoic orogens, except in areas where topography has been rejuvenated by Quaternary glaciations or river incision (Jarman 2006; Ballantyne et al. 2014; Hilger et al. 2018; Böhme et al. 2019). In Europe, this is partly due to the lower topographic relief and less intensive rockslide triggers (e.g. seismicity, river incision) offered by the Palaeozoic mountain belts compared to the Cenozoic alpine ranges. The declining potential to produce large slope instabilities with mountain range lifetimes is termed "stress hardening" (Jarman 2006). This phenomenon is the result of long-term erosion, which gradually removes unstable volumes of rock, and the topography of the mountains is then more in equilibrium with the geological structure. In such areas, rockslides cluster mainly in rejuvenated, more recently cut river valleys or within the youngest glacial breaches (Jarman and Harrison 2019).

However, the interpretation of the origin of these rockslides in the context of landscape evolution has so far been hampered by minimal knowledge about their onset and lifespans. Only for a small number of slow-moving rockslides the length of their evolution has been estimated (Schwartz et al. 2017; Böhme et al. 2019; Hilger et al. 2021; Břežný et al. 2021), and no such data exist for Palaeozoic highlands of Central and Western Europe situated outside the Pleistocene ice limits.

In the crystalline domains of the Bohemian Massif formed by plutonic and metamorphic rocks (Fig. 1), rockslides are extremely rare, in contrast to the sedimentary and volcanic parts of the area (Migoń et al. 2017; Raška et al. 2016). In the Czech part of the Bohemian Massif, only single cases of rockslides in crystalline rocks have been inventoried, exclusively from mountains glaciated during the Last Glacial Maximum (Hartvich and Mentlík 2010), from tectonically more active parts of the area, such as the flanks of the Eger Rift (Burda et al. 2018), or from deeply incised river valleys (Zvelebil et al. 1996). The last group mainly includes river valleys incised to the eastern marginal slope of the Bohemian Massif at the contact with the Alpine–Carpathian foredeep. Although these valleys are only the first few hundred metres deep, they often have steep rock slopes and resemble canyons (Ivan and Kirchner 1994). Several rockslides from these valleys have been described by Hrádek (1998); however, information on their kinematics and chronological time frames is completely lacking.

The present study reveals the predispositions, structure, mechanism and age of the Ledové sluje rockslide (LR), which is some of the most distinct rockslides originating within the nonglaciated Variscan orogenic belt in southeastern Czechia, Central Europe. The rockslide is unique with its remarkably well-preserved morphology as well as accessible internal structure through distinctly developed crevice-type caves (CTCs). Although this rockslide has been studied for more than a century (Filek 1895), there are still controversies regarding its predisposition, triggers, mechanism of movement and especially its age (Špalek 1935; Demek 1996; Kopecký 1996; Zvelebil et al. 1996).

The main goal of this study was (i) to reveal the structural control of the rock massif through structural and geophysical data analyses, (ii) to assess the types of mass movements that formed the studied rockslide and (iii) to present the results of terrestrial cosmogenic nuclides dating outlining the minimum age of the rockslide.

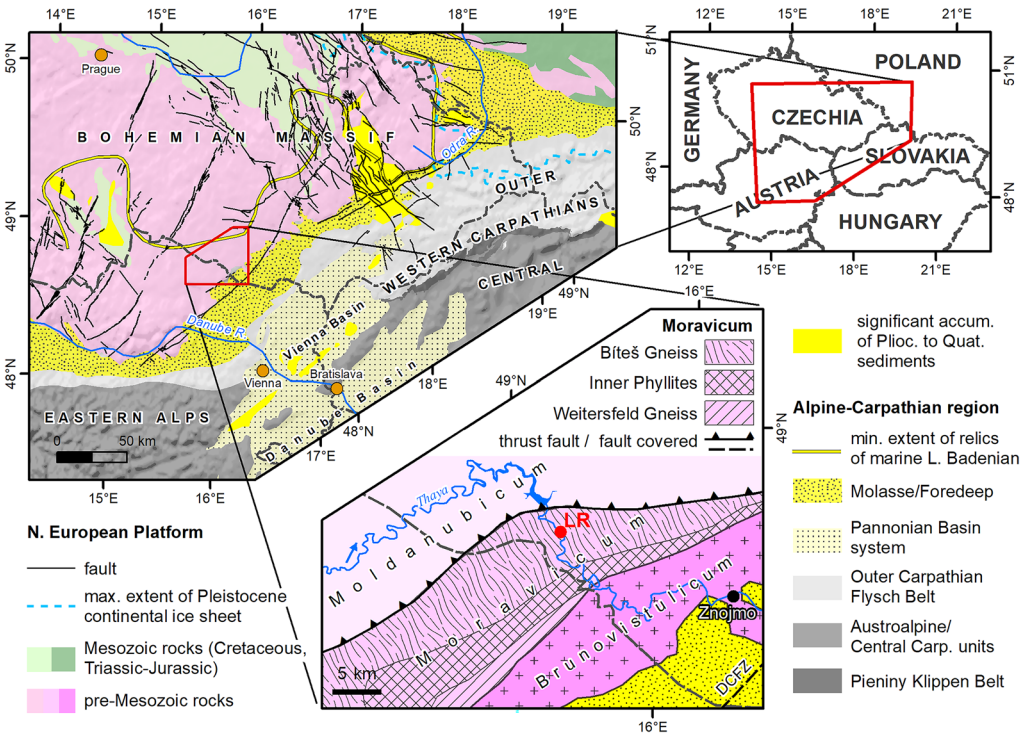

Fig. 1 Simplified geological map of the Alpine–Carpathian–Bohemian Massif junction area (based on Špaček et al. 2015) with the geological setting of the Dyje Window. LR, the Ledové sluje rockslide; DCFZ, Diendorf-Čebín Fault Zone

Combining these approaches, we demonstrate for the first time the long-term evolution of rockslide in the Variscan part of Europe.

Regional settings

Corresponding to the front of the Variscan collisional belt, the eastern margin of the Bohemian Massif is composed of three main tectonically stacked Precambrian and Palaeozoic crystalline complexes. In the W–E direction, the Moldanubicum complex is thrust over Moravicum, and both complexes are jointly thrust over Brunovistulicum (Dudek 1980; Schulmann et al. 1994). Devonian limestones sandwiched between the Brunovistulicum basement and Moravicum complex indicate the Variscan tectonics of the area, more accurately a Lower Carboniferous age of the main tectonic phase (Dallmeyer et al. 1994). Within the Moravicum domain, two tectonic windows — the northern Schwarzawa window and the southern Dyje window — were formed (Suess 1912). In the latter, the Ledové sluje rockslide is located (Fig. 1). The Dyje window (dome), more precisely the tectonic half-window, consists of the lower inner phyllite unit (Suess 1912; Batík 1993) exposing mainly metapelites, gneiss, quartzites and marbles and the higher Bíteš gneiss nappe unit. It contains strongly deformed leucocratic orthogneiss with an expected Cadomian (Late Proterozoic–Cambrian) age, penetrating a varied metasedimentary succession of the outer phyllite unit (Schulmann et al. 1994).

LR is situated in the Znojmo Highland, i.e. a slightly undulating landscape of the Bohemian Massif on the border between Czechia and Austria (Kopecký 1996). Even though the mean altitude of the Znojmo Highland does not exceed 365 m, the southeastern marginal slope of the Bohemian Massif is deeply incised by the Thaya (Dyje *Cze.*) River and other rivers flowing into the adjacent Alpine–Carpathian foredeep. The resulting canyons with often rocky steep slopes reach depths greater than 200 m. Morphotectonic evolution of the area was influenced by the proximity of the Diendorf-Čebín Fault Zone (DCFZ) (Roštínský et al. 2013) (Fig. 1). Manifesting as an ~ 200-km-long NE–SW-trending fault system of predominantly normal and strike-slip character, the DCFZ represents surface expression of the Variscan suture between the Moldanubicum and Brunovistulicum complexes with assumed tectonic activity in the Quaternary (Špaček et al. 2017).

The LR site is situated in the western part of the Thaya River canyon, 40 km upstream from the outlet of the river into the Alpine–Carpathian foredeep. More specifically, it occupies the steep northwestern slope of the incised meander spur, which forms an ~ 800-m-long rocky promontory of the Větrník hill plateau at ~ 500 m a.s.l. (Fig. 2). The slope is composed of the Bíteš orthogneiss, formed by flaser, leucocratic two-mica gneiss (Ivan and Kirchner 1994). Metamorphic foliation dips 15–30° NW in general (Ivan and Kirchner 1994). The mean inclination of the failed slope oscillates at approximately 25° (Košťák 2001) but locally exceeds 55° (Demek 1996). Joint systems strike in the NW–SE, WSW–ESE and NNE–SSW directions, which is also reflected by the shape of the river meanders (Zvelebil et al. 1996).

The LR is not the only slope failure described within the wider area (Hrádek 1998), but with its complexity, it remains unique. Except for typical gravitational features such as undulated terrain with rock scarps or scree slopes, it reveals distinct 100-m-long and 25-m-high fault-predisposed rock wall (locally named the Main Trench) in its upper portion, sagged and rotated rock blocks

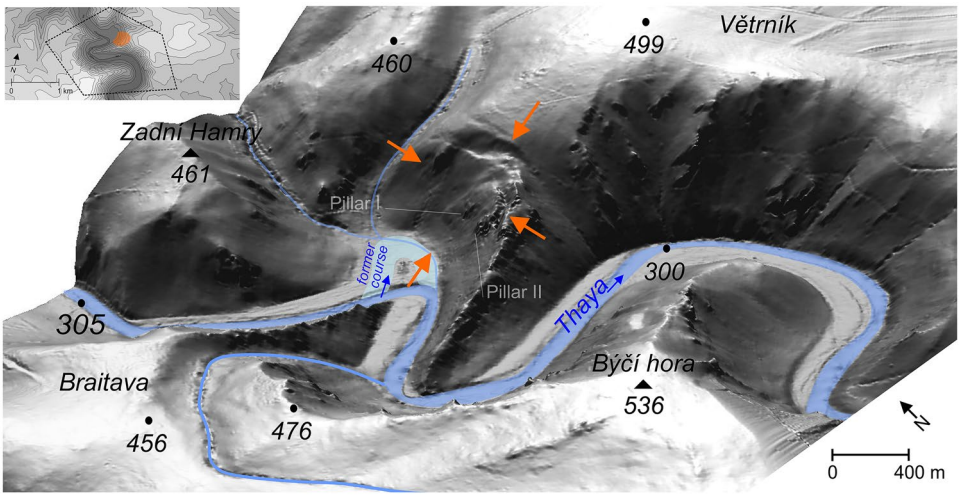

Fig. 2 The Ledové sluje rockslide (delimited by orange arrows) and the Thaya River canyon. Visualization is based on the DMR5G digital elevation model (ČÚZK) with 1-m resolution. Pillars I and II are shown in more detail in Fig. 3

(locally named Pillar I and Pillar II) and pseudokarst caves (both crevice and boulder types) (Figs. 3 and 4). Cave openings along the Main Trench as well as within the pillars and scree accumulations have been described since the nineteenth century (Kopecký 1996). Even though caves reveal complicated morphology, the main direction of their crevice-type corridors (NE–SW) is parallel to the main fault scarp strike. Other shorter cave corridors follow NW–SE or NNW–SSE directions (Kopecký 1996). Until 1996, speleologists documented 7 caves within Pillar I with cumulative length up to 100 m and elevation change up to 20 m and 7 caves within Pillar II with the length more than 400 m and elevation change up to 30 m (Kopecký 1996) (Fig. 3). Wagner (2001) described 17 caves. He highlighted that some individual underground crevices are 10 m high.

Overall, the caves reveal the typical morphology described earlier by Lenart (2015) and Margielewski and Urban (2017) from the Outer Western Carpathians. Individual caves are interconnected through widened joints by visible connection or at least by air draft. Rock surfaces within the caves are covered or impregnated by opal, silicate, phosphate or gypsum coatings (Cílek 1993). Some of the caves are iced during the cold season, which further supports high vertical disruption of the rockslide structure. It is symptomatic that the icing of the caves gave the name of the whole rockslide (Ledové sluje (*Cze.*) = ice caves). From time to time, rock falls are observed (Košťák 2001), both on the surface and inside caves.

Methods

Geomorphic mapping

Geomorphic mapping was focused on landforms related to slope failures, and it was conducted by surface GNSS mapping and speleological surveys inside the crevice-type caves. Geomorphological interpretation was based on the high-resolution LiDAR-derived digital terrain model of the Czech Republic provided by the State Administration of Land Surveying and Cadastre (DMR5G) with a spatial resolution of 1 m and the maximum error in altitude reaching 0.3 m in forested areas. A detailed topographic map at a scale of 1:5 000 was used as the main source for surface mapping, which helped to delimit slope failure and reveal distinct landslide features in the study area. The existing results of geomorphological mapping, research and inventories by Ivan and Kirchner (1994) and Demek and Kopecký (1996), were also considered. Detailed geomorphological maps at scales of 1:5 000 (Demek and Kopecký 1999) and 1:200 (Počta and Schönbeková 1991) served as basic sources for a better understanding of the wider spatial context of the rockslide area. Cave maps obtained earlier by speleologists were used for orientation in CTCs. Within them, we used tape for the identification of vertical shifts indicating sagging of blocks.

Structural analysis and movement mechanism

The rock surfaces exposed mainly within the CTCs were investigated by structural analysis. The methodology by Margielewski and Urban (2003) was used to determine the mass movement types that formed the rockslide. This method relies on the fact that changes in the dip and direction of discontinuities between in situ rock masses and gravitationally shifted blocks reveal the type of local gravitational movement, i.e. translation, toppling or horizontal and vertical rotations of rock packets (sensu Dikau et al. 1996). This assumption is valid only in spatially limited slope sections (~ 10^1 m) and for rock masses not affected by folding. Measured in dip direction/dip angle format for planes and trend/plunge format for lines, structural data of faults, fractures and foliation planes have been visualized as contour diagrams in the lower hemisphere of the Lambert equal area projection.

Electrical resistivity tomography

The geoelectrical properties of the rock massif were examined by means of a multielectrode resistivity measurement technique, i.e. electrical resistivity tomography (ERT). The survey was conducted to reveal the internal structure of the main scarp area of the studied rockslide. Measurements are based on direct current passing through a pair of electrodes grounded to the subsurface and on measured potentials on a pair of potential electrodes (Milsom and Eriksen 2011). According to Ohm's law and the geometric factor

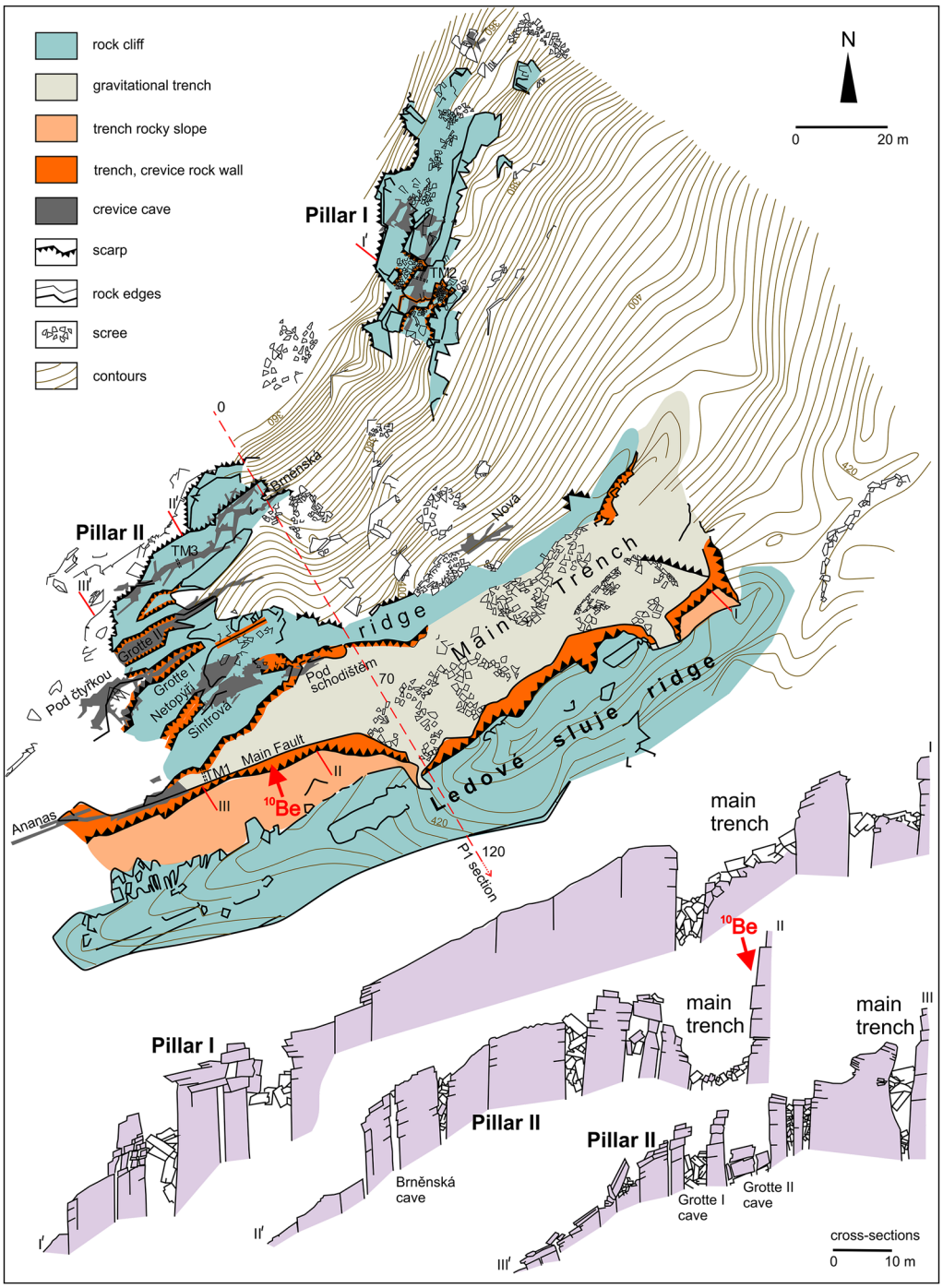

Fig. 3 Detailed geomorphology of the most distinct portion of the Ledové sluje rockslide (after Počta and Schönbeková 1991) with caves, cross-sections (after Zvelebil et al. 1996) and ERT Section P1 with stationing. ^{10}Be, position of TCN dating profile; TM, positions of extensometric measurements (Košťák 2001)

(k coefficient), the apparent resistivity (ρ_a) is then calculated and further recalculated into real resistivity (ρ) by means of an inversion procedure in Res2Dinv software (Loke and Barker 1996). The resulting inverted models are depicted as resistivity sections.

Two ERT sections were measured using a multielectrode system ARES (GF Instruments, Czechia). Both profiles were conducted in a Wenner-Schlumberger array with a 5-m electrode spacing. Section P1 was 165 m long, and Section P2 was 185 m long.

Surface exposure dating

Terrestrial cosmogenic nuclide (TCN) dating using ^{10}Be was used to determine the minimum age of the main 15-m-high scarp of the rockslide. The method is based on a concentration measurement of in situ produced cosmogenic nuclides that builds up in the mineral's lattice from interactions occurring between the target mineral and particles arising from secondary cosmic ray flux (for

Fig. 4 Morphology of the most distinct portion of the Ledové sluje rockslide. **a** The main scarp with positions of rock sampling for TCN dating; **b** the main scarp above the Main Trench filled with blocks; **c** the highly disrupted front of Pillar II with the entry into the Brněnská crevice-type cave; **d** the interior of the Brněnská crevice-type cave with typical rectangular corridors filled with wedged blocks; **e** narrow crevice in Brněnská cave with apparent vertical shift of the opposite blocks indicating sagging. See Fig. 3 for the TCN dating profile position and names of individual caves

further details, see, e.g. Ivy-Ochs and Kober 2008). Recently, dated landslide scarps testified to the usefulness of this dating strategy for determining the timing of scarp exposure (e.g. Le Roux et al. 2009; Zerathe et al. 2014; Schwartz et al. 2017).

Samples for ^{10}Be dating were taken from the nearly vertical main scarp with minimal evidence of secondary rockfalls, subsequent weathering and postfailure erosion in general. For assessment of different phases of possible slowly moving rockslide, a total of four rock samples placed one above the other along the transect on the subvertical scarp surface were obtained (Fig. 4a).

All samples were crushed, sieved and cleaned with a mixture of HCl and H_2SiF_6. The extraction method (Braucher et al. 2000; Merchel and Bremser 2004) for ^{10}Be involves isolation and purification of quartz and elimination of atmospheric ^{10}Be. Exactly 150 µl of a (3025 ± 9) ppm ^{9}Be solution was added to the decontaminated quartz. Beryllium was subsequently separated from the solution by successive anionic and cationic resin extractions (DOWEX 1X8 then 50WX8) and precipitations. The final precipitates were dried and heated at 800 °C to obtain BeO and finally mixed with niobium powder prior to measurements, which were performed at the French AMS National Facility, ASTER, located at CEREGE in Aix-en-Provence. Beryllium data were calibrated directly against the STD11 standard (Braucher et al. 2015) with a ^{10}Be/^{9}Be ratio of $(1.191 \pm 0.013) \times 10^{-11}$. Analytical uncertainties (reported as 1σ) include uncertainties associated with AMS counting statistics, AMS external error (0.5% for ^{10}Be) and chemical blank measurement.

A sea-level high-latitude spallation production rate of 4.02 ± 0.32 at. g^{-1} a^{-1} (Borchers et al. 2016) was used and scaled using Stone (2000) polynomials.

The general equation used to model ^{10}Be concentrations considering the three types of particles involved is given by Eq. 1:

$$N(0,\varepsilon,t) = \frac{P_n.e^{-\frac{\rho x}{\Lambda_n}}.\left(1-e^{\left(-t\left(\frac{\rho\varepsilon}{\Lambda_n}+\lambda\right)\right)}\right)}{\frac{\rho\varepsilon}{\Lambda_n}+\lambda} + \frac{P_{slow}.e^{-\frac{\rho x}{\Lambda_{slow}}}.\left(1-e^{-t\left(\frac{\rho\varepsilon}{\Lambda_{slow}}+\lambda\right)}\right)}{\frac{\rho\varepsilon}{\Lambda_{slow}}+\lambda} + \frac{P_{fast}.e^{-\frac{\rho x}{\Lambda_{fast}}}.\left(1-e^{-t\left(\frac{\rho\varepsilon}{\Lambda_{fast}}+\lambda\right)}\right)}{\frac{\rho\varepsilon}{\Lambda_{fast}}+\lambda} + N(x,\varepsilon,\infty).e^{-\lambda t} \quad (1)$$

where P_{n}., P_{stop}. and P_{fast} are the production of neutrons, stopping and fast muons, respectively; ρ is the material density; ε is the denudation rate; t is time; and Λ_{neut} and $\Lambda_{stop.}$ and Λ_{fast} are the attenuation lengths of neutrons (150 g/cm²), stopping (1500 g/cm²) and fast muons (4320 g/cm²), respectively. λ is the radioactive decay constant (λ = ln2/half-life). x is the depth before the sliding event (after the sliding event, samples are exposed at the surface).

The muon contribution scheme follows Braucher et al. (2011). Topographic shielding was determined using Dunne et al. (1999).

The term $N(x, \varepsilon, \infty)$ is the inheritance coming from a previous exposure at depth and assuming steady state (T = infinite) and with a denudation ε. This denudation ε is a local long-term denudation rate determined using the top reference samples not affected by the sliding event. The age calculation was therefore a three-step calculation: (i) determination of the long-term denudation rate with the top sample (LS0); (ii) estimation of the inheritance at depth of samples below LS0 assuming the denudation rate determined above; and (iii) determination of the exposure ages after the sliding event considering inheritance determined in step 2.

Results

Geomorphology and structural setting of the rockslide

The LR occupies an area of ~ 0.1 km², with a topographic relief of ~ 150 m. It reveals fresh topography. The upper easternmost portion reveals a typical scarp with a linear and transversely asymmetrical shallow depression/graben separating the rockslide from Větrník Hill (Fig. 2). The northern branch of the failure is topographically rather indistinct, except for Pillar I, revealing rock walls and rock towers highly disrupted by a system of open fissures and CTCs (Fig. 3). There, the original rock structure is strongly overprinted by varied secondary failures — rock falls, slides and rotations. Below Pillar I, the slope is covered by scree accumulation.

The southern branch of the LR is very distinct. From the Ledové sluje ridge, Pillar II is separated by the gravitational trench (the Main Trench) bounded by vertical rock walls or steeply declining scree piles (Fig. 3). Downslope, NE–SW elongated deep opened fissures and CTCs separate blocks of the failed rock mass. Pillar I culminates with a highly disrupted northwestern rock face with the entrances into the largest CTC — the Brněnská cave (length ~ 400 m). The lower part of the slope is covered by scree cover. Overall, the foot of the LR lacks a distinct toe due to the erosion of the Thaya River that shaped the formerly incised meander (Fig. 2).

Viewed from the caves, we found that the orthogneiss rock mass was highly heterogenous. In addition to joints and faults, we detected subvertical mineral veins (~ 10^1 cm thickness) and subhorizontal intercalations (~ 10^1 cm). Additionally, weak, weathered and eroded layers (~ 5–13 cm thick) permeating the massif equate to biotitic paragneiss inclined 2–4° within the overdip slope (sensu Meentemeyer and Moody 2000), earlier described by Košťák (2001). Tectonic features such as Riedel shears, plumose structures, tectonic mirrors and striations were observed on rock walls.

The main structural control of the rock massif (Fig. 5) corresponds mainly to NE- to ENE-striking steep fractures and faults, predominantly facing the SE (contour maximum density 145/83). Metamorphic foliation gently dips towards the NW (maximum 300/5). Identified mainly on the basis of striation surfaces and tectonic mirrors, faults are characterized primarily by ENE-striking (maximum 334/83) and secondarily also WNW-striking (197/86) structures with SW-oriented striations with dip range 30–80° (maximum 240/63).

The eight CTCs (the *Ananas*, *Grotte 1*, *Grotte 2*, *Netopýří*, *Sintrová*, *Pod schodištěm*, *Nová* and *Brněnská Caves*) and the Main Trench were analysed based on changes in the anisotropy of upslope and downslope rock blocks. The structural assessment avoided sites with locally folded orthogneisses since their anisotropy is attributed to continuous tectonic strain in rocks, not to rigid deformation formed by slope failure.

The extensive structural analysis of upslope and downslope blocks enabled the identification of translated and rotated blocks within the rockslide body. The structural sketch showing the foliation within all analysed sites is shown in Fig. 6. Recalculated into apparent dips, the representative foliation planes are also depicted in the NW–SE-directed pseudosection (Fig. 6). The translated blocks exert identical fabric with foliation planes dipping gently to the NW (300/5). The rotated structures are characterized mainly as back-rotated, with foliation dipping SE up to 11° (except *the Grotte 1 Cave*), while toppled blocks dip to NW up to 16–22° (the *Nová*, *Ananas*, *Brněnská Caves*).

Resistivity imaging

Figure 7 shows the measured ERT profiles and their locations within the LR area. Absolute values of resistivity of both sections were strongly influenced by highly resistive orthogneiss.

The P1 section oriented in the NW–SE direction was measured across the main ridge above the Main Trench downwards behind the lowermost known crevices of the Brněnská Cave. The most striking feature of the P1 section is represented by the high resistivity domain at stationing ca. 70–100 m, exceeding 10,000 Ω·m. It is interpreted as a relatively fresh compact rock mass exposed by the main scarp of the rockslide with a near-surface zone of distinct resistivity variations. From SE at stationing ca. 90 m, it is bordered by a sharp resistive transition steeply dipping towards the SE, which is interpreted as a fault structure predisposing the Main Trench. Down the slope, up to ~ 12-m-thick surface domain of relatively low resistivity (< 3000 Ω·m) may be tracked at stationing 25–65 m, acting as a relaxed part of the rock massif with slided blocks separated by crevices.

Oriented SW–NE, the P2 section runs parallel to the Main Trench and further upwards through the N–S-directed shallow trench. The profile clearly captured its subsurface structure and documents gravitational breakup of the highest portion of the rockslide. The subhorizontal zone of reduced resistivities (< 600 Ω·m) is well pronounced at stationing from ca. 65 m onwards with a base situated 15 m deep. This domain propagates up to the surface at stationing 80–100 m, corresponding with the expressive topographic response of the gravitational trench.

Dating

All dated samples from the 15-m-high rock wall of the main rock scarp show Late Pleistocene exposure ages, specifically falling in the younger half of the Last Glacial period (Tables 1 and 2). The uppermost sample LS1 yields an age of 42.6 ± 4.4 ka, the middle sample LS2 yields an age of 26.6 ± 3 ka, and the lowermost sample LS3 reveals an age of 23.4 ± 2.7 ka. As the ages decrease from the top to the bottom, the rockslide formed due to slow gradual or multievent displacement over tens of thousands of years rather than during a single catastrophic event.

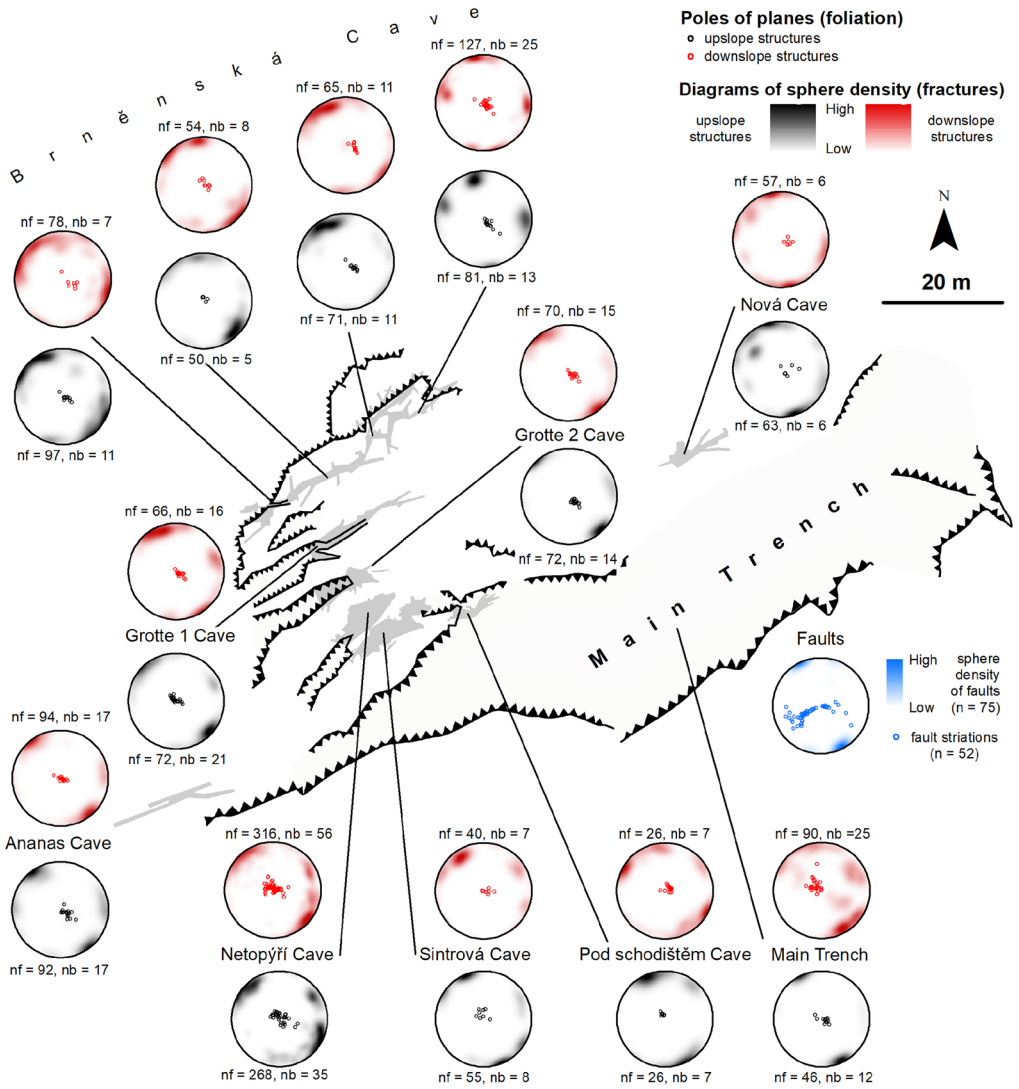

Fig. 5 The results of structural analysis reveal mutual relations between upslope (black diagrams) and downslope (red diagrams) rock blocks, predisposition and types of slope movement, number of measured faults and striations (n), fractures (nf) and foliation planes (nb)

Discussion

Causes and triggers of the rockslide

The Ledové sluje rockslide belongs to the most explored slope failures in Central Europe with a long tradition of investigation. The authors of the first descriptive studies outlined the crucial triggering role of the Thaya River undercutting the slope (Filek 1895; Špalek 1935). As summarized by Demek (1996), various authors also mentioned the crucial role of weak biotitic paragneiss intercalations and Pleistocene frost weathering as predisposing and preparatory factors. Kopecký (1996) underlined the influence of local folding and jointing.

Our investigation also revealed other potential geological predispositions of slope instability — subvertical mineral veins.

Based on the analysis of nearly 3000 structural measurements, we determined the overall pattern of steep NE- to ENE-striked fractures and faults protruding into a highly incoherent rock massif. A similar structural pattern was previously described by Zvelebil et al. (1996), who also pointed out the significance of NW- and NNE-trending fracture sets. NE-striking structures are developed longitudinally with respect to the strike of gently dipping foliation planes. Pospíšil and Pazdírek (1998) highlighted the importance of NW-trending fractures and faults, which was also supported by the study of regional fracture pattern (Pospíšil et al. 1997). They found the transverse NW-directed fabric to be the main predisposition that enabled the development of longitudinal fissures and therefore the subsequent evolution of the rockslide. Such a structural setting of the rock massif, together with the position of the rockslide predominantly on a NW-oriented overdip slope (sensu Meentemeyer and Moody 2000), defines the main predisposing factors for the development of LR and respective CTCs.

As summarized by Ivan and Kirchner (1994), undercutting caused by the former Thaya River course remains the suspicious triggering factor. As a result of the DEM visualization (Fig. 2), the foot of the LR is obviously eroded, and the accumulation part is

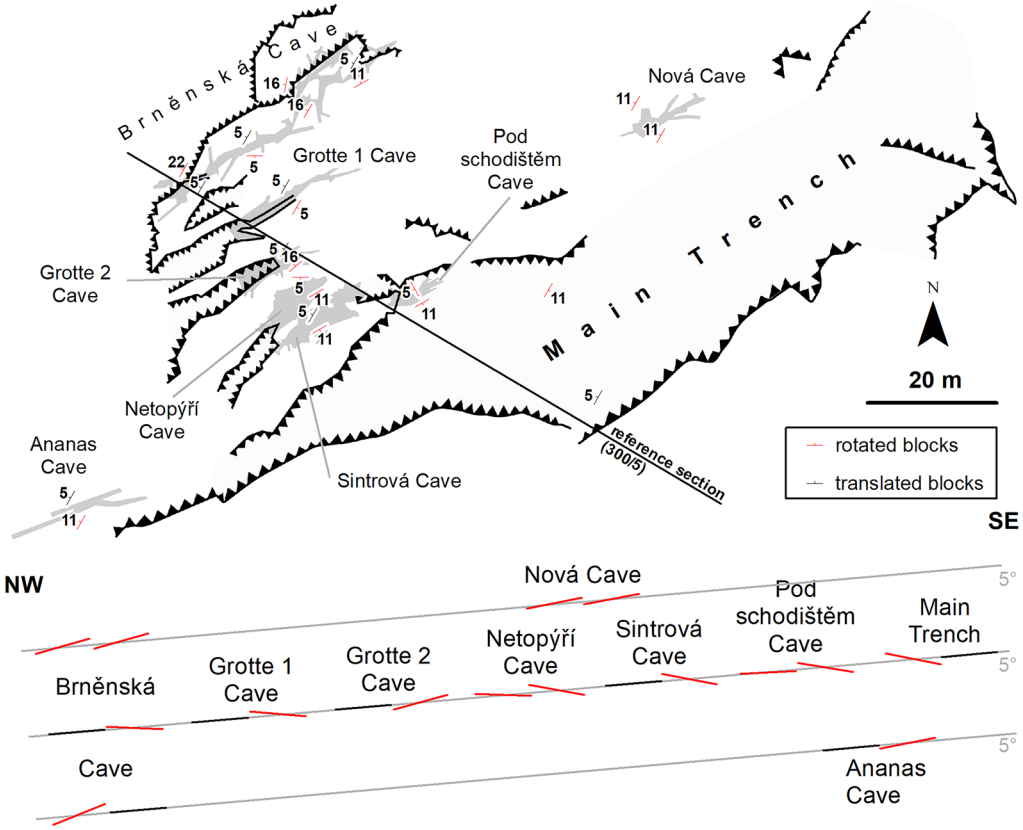

Fig. 6 Top, structural map revealing the geometry of translated (black marks) and rotated (red marks) rock blocks within the rockslide body; bottom, NW–SE-oriented reference pseudosection indicating the clustering of the rotated blocks with respect to the translated blocks. See the reference section above

apparently missing. Based on ground penetrating radar profiles, Hubatka (2001) revealed a former channel within the incised meander buried beneath a 20–30-m-thick cover of colluvial deposits at the foot of the rockslide.

In contrast, Zvelebil et al. (1996) assumed tectonic impulse for at least the initial evolution stages of the LR. Pospíšil and Pazdírek (1998) also mentioned the importance of a seismic factor, although without providing any clear evidence. The proximity of the DCFZ has often been argued to support the hypothesis of a seismic trigger. The southern section of the DCFZ near Krems and Melk in Austria is characterized by weak recent seismicity with an estimated maximum magnitude $M_w \sim 3.5$ (Lenhardt et al. 2007; Špaček 2021). The Ried am Riederberg earthquake in 1590, known as the strongest historical earthquake in Austria with an estimated magnitude $M_w \sim 5.8$ and an epicentral intensity of 9° EMS-98 (Hammerl and Lenhardt 2013; Hammerl 2017), is located ~ 70 km from the LR site. A few instrumentally or macroseismically recorded earthquakes are also known from less distant areas (< 30 km from the LR site), e.g. from Hostěradice ($M_L = 2.5$; years 2000 and 2014), Božice ($M_L = 1.4$; year 2006) or Ctidružice ($M_L = 0.9$; year 2018; ~ 10 km from the LR site; Špaček 2021). However, these earthquakes appear to be too weak to trigger a coherent deep-seated rockslide, generally requiring M > 4.5–5 (Murphy 2015).

Subsurface structure of the rockslide

Joint interpretation of outcrop and geophysical data can significantly improve the understanding of the internal structure of the rock mass (Place et al. 2016; Lesage et al. 2019; Müller et al. 2020). Likewise, structural analysis can enhance the interpretation of geophysical data characterizing mass movement features (Břežný et al. 2018; Chalupa et al. 2018; Tábořík et al. 2017), even much better if performed in CTCs. However, due to the rare occurrence of accessible CTCs in landslide terrains, such studies are sparse (Pánek et al. 2010).

The studied rockslide is characterized by a series of disrupted slided blocks separated from each other by fractures and crevices or within its upper part by topographically distinctive gravitational trenches, which clearly correlate with relatively low-resistivity or high-gradient domains of the resistivity sections (Fig. 7). However, high resistivity values represent a coherent rock massif without fracturing that was exposed by the main scarp of the rockslide. The contrasting resistivity response resembles the geophysical image described by Heincke et al. (2010) from similar conditions of the Åknes rockslide developed in gneissic rocks in Norway. Based on an integrated 3D geophysical survey, the authors have shown that similar high resistivity zones (> 17,500 Ω·m) can be assigned to intact and unfractured rock masses with low water content.

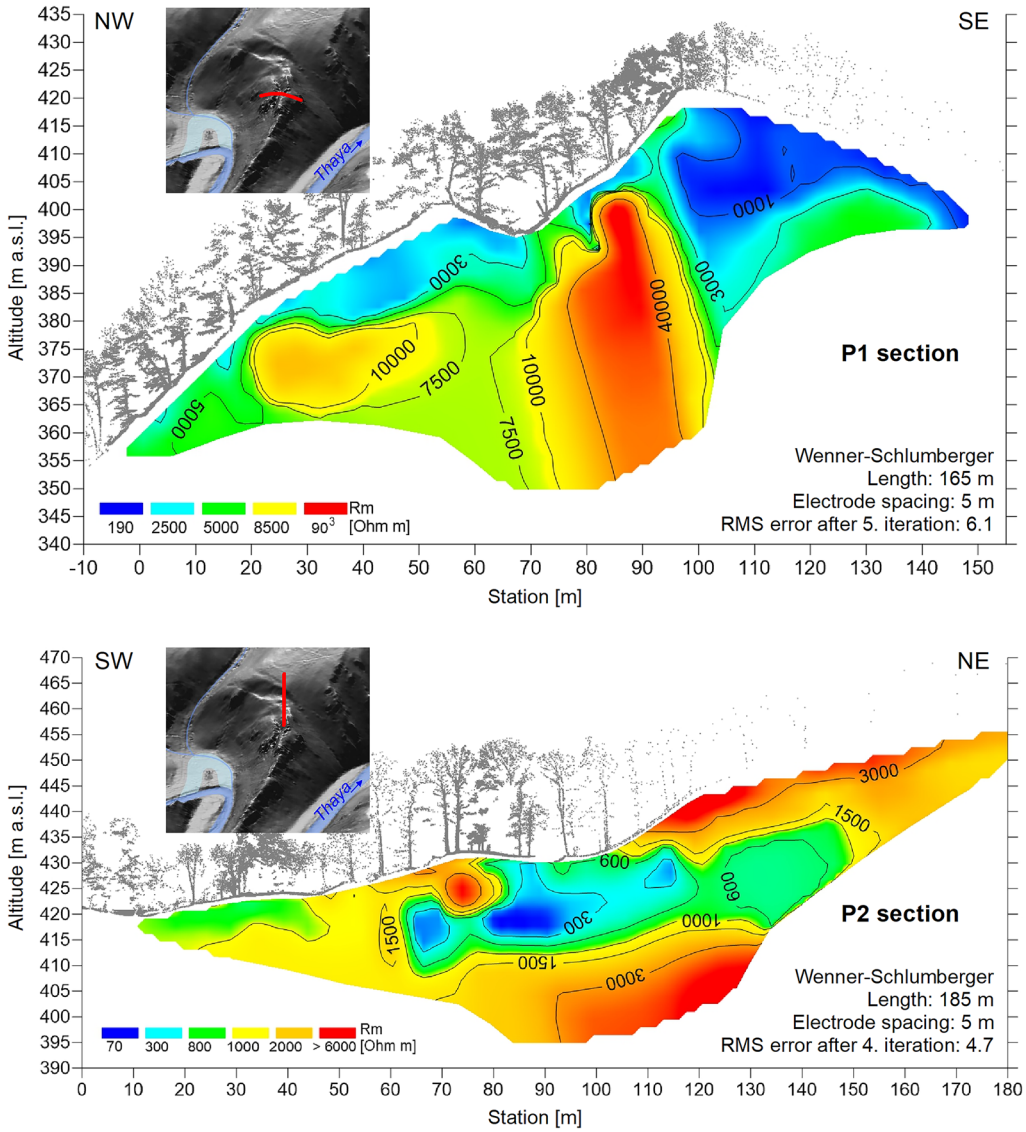

Fig. 7 ERT sections P1 and P2 and their locations within the rockslide

Neither of the two P1 and P2 profiles revealed a distinct sliding surface (Fig. 7). However, the topmost sliding surface is expected to occur at depths of 12–15 m based on the interpretation of resistivity Section P1. Within the P2 section, the sliding surface that probably enabled the evolution of the distinct N–S trending trench could be 20 m deep. The previous geoelectric surveys conducted by Pospíšil and Pazdírek (1998) and Hubatka (2001) indicated the disruption of the rock massif to depths over 35 m and the occurrence of the

Table 1 Measured sample properties. The depth is the vertical distance from the sample to the top of the scarp. The shielding is the actual topographic shielding. See Fig. 4 for the locations of the samples

Sample	Depth (cm)	Shielding	Mass quartz	^{9}Be added	^{10}Be/^{9}Be	Uncertainty	^{10}Be (at/g)	^{10}Be uncertainty (at/g)
LS0	0	0.709	15.5213	3.137E+19	8.59300E-14	8.1200	169 381	13 754
LS1	500	0.487	19.8964	3.248E+19	5.67016E-14	6.4000	89 099	5 702
LS2	950	0.487	22.5354	3.135E+19	5.00084E-14	7.7011	66 612	5 130
LS3	1450	0.452	24.9253	3.234E+19	4.42379E-14	7.9844	54 640	4 363
Blank	-	-	-	3.153E+19	2.12776E-15	17.4937	-	-

Table 2 Exposure ages and inheritance of scarp samples. See Fig. 4 for the locations of the samples

Sample	Shielding at depth	Long-term denudation rate	Inheritance (At/g)	Exposure age (ka)
LS0	0.709	17.0 ± 1.4 m/Ma	169 381	Reference
LS1	0.709		22 793	42.6 ± 4.4
LS2	0.709		16 994	26.6 ± 3
LS3	0.709		12 460	23.4 ± 2.7

main sliding surface at depths of 18–20 m. This is in accordance with the maximal depth of the explored CTCs, which reaches 30 m (Kopecký 1996).

Mechanism of the movement

The mechanism of rock slope failure was previously interpreted as a large rock fall (e.g. Filek 1895; Koutek 1934 and others) or gravitational spreading (Kirchner and Ivan 1994). Based on measurement by a tape extensometer, Zvelebil et al. (1996) speculated about deep-seated gravitational movement, manifested by up to 3 mm of cumulative shift during 3 years of investigation. They concluded that the initial failure may be of catastrophic origin. Demek (1996) proposed the scenario of slope failure development as follows: (i) incision of the Thaya River, (ii) stress release and formation of joints parallel to slope, (iii) deep-seated sliding surface development and gravitational widening of tension cracks, including the influence of frost weathering and (iv) subsequent slow-moving rockslide and rock falls.

Our structural analysis revealed a clear pattern of identically oriented slided rock blocks repeating over the rockslide. These blocks with NW-oriented gently inclined foliation (300/5) are regarded as translated. Along the displayed reference section (Fig. 6), they alternate with rotated blocks as well. This slope structure is interpreted to be formed during the release of horizontal stress caused probably by the incision of the river canyon (Stead and Eberhardt 2013; de Blasio 2011). Identically oriented translated blocks indicate that deformation occurred along the planar sliding surface. The rotated blocks seem to be a result of spatially constrained back-rotation movements within the rockslide. However, the peripheral rock blocks outside the reference line tend to be toppled rather than back-rotated.

The mechanism of rock slope movement could be refined in the future using slope stability modelling (Stead and Eberhardt 2013; Azarafza et al. 2021), namely, by combining simple kinematic analysis (Brideau et al. 2009) and more advanced discontinuum modelling (He et al. 2022). Time-dependent modelling (e.g. Riva et al. 2018) can help to understand the long-term progressive evolution of the rockslide from its nucleation to the evolution of the sliding surface in relation to the history of river valley incision and lateral shifts of the Thaya River.

Chronological context of the rockslide

Very few landslides have been dated in the pre-Cenozoic mountains, and the LR represents the first ^{10}Be dated rockslide in the Variscan orogenic belt of Europe (Pánek 2019). Since we do not know the rate of erosion of the rock face and are unable to determine the exposure time of the upper 5 m of the scarp, the obtained age of the rockslide should be considered the minimum (Lang et al. 1999). If we simply extrapolate towards the top edge of the scarp the exposure time between the uppermost samples LS1 and LS2, we obtain an initiation of rockslide between ~ 48 and 73 ka. However, this extrapolation must be taken with caution because the exposure of the scarp was not linear according to the observed age of the samples. Using the central ages, the average slip rate between LS1 and LS2 was 0.28 mm/year, while between LS2 and LS3, it was 1.56 mm/year. However, the uncertainty margins of the ages for the lower samples overlap, so it cannot be ruled out that the lower 5 m of the scarp was exposed instantaneously.

Due to the lack of rock surfaces in the northern portion of LR, the TCN dating does not allow determination of the entire life span of the rockslide. In any case, the majority (~ 10 m) of the dated scarp was exposed in the Last Glacial during marine isotope stages (MIS) 3 and 2, between ~ 43 and 23 ka. Such an old age is rather exceptional for landslides with a recent morphological fingerprint, as > 95% of the global set of dated landslides show a younger age (Pánek 2019). This may be because most landslides to date have been dated in higher, tectonically mobile mountain ranges with high erosion rates (Korup et al. 2007). In contrast to the LR, which has a distinct morphology, landslides dated to the Late Pleistocene in the surrounding areas built by sedimentary rocks have been identified only from sedimentary records and are no longer morphologically apparent (Pánek et al. 2014; Špaček et al. 2017; Jankovská et al. 2018). We explain this by the higher rock mass strength of the orthogneiss, which allows longer topographic survival of the rockslide.

The origin of most landslides in central Europe is related to the wetter climatic phases of the Holocene or Late Glacial (Starkel et al. 2013). Correlations with palaeoclimatic proxy data are more difficult for the Last Glacial because only a few landslides were dated to this period. However, only three dated pre-Last Glacial Maximum (LGM) landslides from the eastern part of Czechia formed at approximately 50 ka in warmer and more humid interpleniglacial conditions of MIS3 (Pánek et al. 2014; Špaček et al. 2017; Jankovská et al. 2018). Although the onset of the Ledové sluje rockslide falls within the same period, its climatic trigger is questionable because its movement continued into the LGM, which was characterized by a dry and cool climate in this region (Antoine et al. 2013). Although the rockslide may have been initiated by higher pore pressures or greater erosive power of the Thaya River during MIS 3, its development continued later, apparently independent of climate, and was more likely dictated by shifts in the river channel and related lateral erosion (Fig. 2).

Additionally, the LR still reveals recent activity. Between 1992 and 2001, Košťák (2001) recorded recent movements within open fissures and CTCs using the optical–mechanical crack gauge TM-71, which

enables measurements in three axis directions (Klimeš et al. 2012). The positions of the extensometric measurements are marked in Fig. 3. The TM1 station detected an overall 0.4 mm subsidence of the downslope situated block. The TM2 station revealed rather complex development. In the period up to the 1997 flood in the study area (Kundzewicz 2007), the rock wall of the upper block dropped by 0.4 mm. After this year, both opposite walls settled around zero again, and the lower block subsided 0.4 mm and slightly shifted horizontally, together with the slight widening of the crevice. The TM3 station revealed an overall subsidence of the upslope rock wall of 1.2 mm. However, it should be assumed that both opposite walls subsided, as proven by our tape measurement. The same station measured slight widening of the crevice and horizontal shift of the lower situated block. In the same period, Zvelebil et al. (1997) summarized the results of precise tape extensometry conducted within the superficial zone of the LR. It showed a movement rate close to 1 mm/year.

Košťák (2001) concluded that the whole-rock block structure is in permanent slow movement and speculated about the influence of active tectonics. Zvelebil et al. (1997) noted that the observed recent movements are surprisingly low in a rockslide with such an apparently fresh topography.

Although LR does not recently represent a major hazard due to its slow movement and remote location, its acceleration in the future cannot be ruled out in the context of the tendency of increasing flood discharges in Central European rivers (Blöschl et al. 2019). Although the Thaya River discharges are regulated by a reservoir located upstream, even relatively small changes in the channel towards the LR could increase the shear stress in the rock slope and cause its possible failure.

Conclusion

The Ledové sluje rockslide is a unique and infrequent slope failure developed in the crystalline Variscan orogen. It manifests fresh topography with rocky trenches, rock walls, slided blocks, scree slopes and crevice-type caves. The rockslide is predisposed chiefly by NE- to ENE-trending steep fractures and faults and NW-oriented gently dipping foliation planes. Our structural measurements show that gravitational deformation of the rock mass occurred along a planar sliding surface, although back rotations and topples occurred locally. Terrestrial cosmogenic nuclide dating of the main rock scarp revealed that the majority of the scarp was exposed in the Last Glacial during Marine Isotope Stages (MIS) 3 and 2 between ~ 43 and 23 ka, which indicates slow gradual or multievent movement of the rockslide rather than a single catastrophic event. However, the onset of rockslide and whether it developed episodically or as a rock mass creep remains uncertain. In any case, the minimum age of LR shows that topographic fingerprints of rockslides developed in crystalline Palaeozoic uplands may preserve an order of magnitude longer than that in the Alpine environment or in landscapes developed in sedimentary rocks. Similar rockslides developed in European Palaeozoic orogens evolved exclusively in areas with rejuvenated topography. This is also a case of the Ledové sluje rockslide, where rejuvenation is driven by the incision of the Thaya River canyon and changes in its former river channel.

Recent slow mass movements may indicate that the original trigger for the rockslide, which was undercutting the slope, is no longer active because the river has already abandoned its original meander loop. A better understanding of the chronology of the Thaya River channel and the use of time-dependent rock slope modelling could in the future help to better understand the evolution of the rockslide in relation to river valley incision and past lateral channel migration.

Funding

Open access publishing supported by the National Technical Library in Prague. This study was supported by the project of the University of Ostrava SGS01/PřF/2022 and the project of VSB — Technical University of Ostrava SP2022/53. G. Aumaître and K. Keddadouche are thanked for their valuable help in AMS measurements; ASTER AMS national facility (CEREGE) is supported by INSU/CNRS and IRD.

Declarations

Competing interests The authors declare no competing interests.

References

Antoine P, Rousseau DD, Degeai JP, Moine O, Lagroix F, Kreutzer S, Fuchs M, Hatté C, Gauthier C, Svoboda J, Lisá L (2013) High-resolution record of the environmental response to climatic variations during the last interglacial–glacial cycle in Central Europe: the loess-palaeosol sequence of Dolní Věstonice (Czech Republic). Quatern Sci Rev 67:17–38. https://doi.org/10.1016/j.quascirev.2013.01.014

Azarafza M, Akgün H, Ghazifard A, Asghari-Kaljahi E, Rahnamarad J, Derakhshani R (2021) Discontinuous rock slope stability analysis by limit equilibrium approaches – a review. Int J Digit Earth 14:1918–1941. https://doi.org/10.1080/17538947.2021.1988163

Ballantyne CK, Sandeman GF, Stone JO, Wilson P (2014) Rock-slope failure following Late Pleistocene deglaciation on tectonically stable mountainous terrain. Quatern Sci Rev 86:144–157. https://doi.org/10.1016/j.quascirev.2013.12.021

Batík F (1993) Geological map of the Podyjí National Park 1 : 25 000. ČGÚ Praha. (in Czech)

Blöschl G, Hall J, Parajka J, Perdigão RAP, Merz B, Arheimer B, Aronica GT, Bilibashi A, Boháč M, Bonacci O, Borga M, Čanjevac I, Castellarin A, Chirico GB, Claps P, Fiala K, Frolova N, Gorbachova L, Gül A, Hannaford J, Harrigan S, Kireeva M, Kiss A, Kjeldsen TR, Kohnová S, Koskela JJ, Ledvinka O, Macdonald N, Mavrova-Guirguinova M, Mediero L, Merz R, Molnar P, Montanari A, Murphy C, Osuch M, Ovcharuk V, Radevski I, Rogger M, Salinas JL, Sauquet E, Šraj M, Szolgay J, Viglione A, Volpi E, Wilson D, Zaimi K, Živković N (2019) Changing climate both increases and decreases European river floods. Nature 573:108–111. https://doi.org/10.1038/s41586-019-1495-6

Böhme M, Hermanns R, Gosse J, Hilger P, Eiken T, Lauknes TR, Dehls JF (2019) Comparison of monitoring data with paleo–slip rates: cosmogenic nuclide dating detects acceleration of a rockslide. Geology 47:339–342. https://doi.org/10.1130/G45684.1

Borchers B, Marrero S, Balco G, Caffee M, Goehring B, Lifton N, Nishiizumi K, Phillips F, Schaefer J, Stone J (2016) Geological calibration of spallation production rates in the CRONUS-Earth project. Quat Geochronol 31:188–198. https://doi.org/10.1016/j.quageo.2015.01.009

Braucher R, Bourlès DL, Brown ET, Colin F, Muller JP, Braun JJ, Delaune M, Edou Minko A, Lescouet C, Raisbeck GM, Yiou F (2000) Application of in situ-produced cosmogenic 10Be and 26Al to the study of lateritic soil development in tropical forest: theory and examples from Cameroon and Gabon. Chem Geol 170:95–111. https://doi.org/10.1016/S0009-2541(99)00243-0

Braucher R, Guillou V, Bourlès DL, Arnold M, Aumaître G, Keddadouche K, Nottoli E (2015) Preparation of ASTER in-house 10Be/9Be standard solutions. Nucl Instrum Methods Phys Res, Sect B 361:335–340. https://doi.org/10.1016/j.nimb.2015.06.012

Braucher R, Merchel S, Borgomano J, Bourlès DL (2011) Production of cosmogenic radionuclides at great depth: a multi element approach. Earth Planet Sci Lett 309:1–9. https://doi.org/10.1016/j.epsl.2011.06.036

Brideau MA, Yan M, Stead D (2009) The role of tectonic damage and brittle rock fracture in the development of large rock slope failures. Geomorphology 103:30–49. https://doi.org/10.1016/j.geomorph.2008.04.010

Březný M, Pánek T, Lenart J et al (2018) Sackung and enigmatic mass movement folds on a structurally-controlled mountain ridge. Geomorphology 322:175–187. https://doi.org/10.1016/J.GEOMORPH.2018.09.004

Březný M, Pánek T, Braucher R, Šilhán K, Chalupa V, Lenart J, Tábořík P. Team A (2021) Old but still active: > 18 ka history of rock slope failures affecting a flysch anticline. Landslides 18:89–104. https://doi.org/10.1007/s10346-020-01483-7

Burda J, Veselý M, Řehoř M, Vilímek V (2018) Reconstruction of a large runout landslide in the Krušné hory Mts. (Czech Republic). Landslides 15:423–437. https://doi.org/10.1007/s10346-017-0881-0

Chalupa V, Pánek T, Tábořík P et al (2018) Deep-seated gravitational slope deformations controlled by the structure of flysch nappe outliers: insights from large-scale electrical resistivity tomography survey and LiDAR mapping. Geomorphology 321:174–187. https://doi.org/10.1016/J.GEOMORPH.2018.08.029

Cílek V (1993) The investigation of crystalline limestone area in National Monument Podyjí, southern Moravia. Speleo 13:16–19 (in Czech)

Dallmeyer DR, Fritz H, Neubauer F, Urban M (1994) 40Ar/39Ar mineral age controls on the tectonic evolution of the southeastern Bohemian Massif. Pre-alpine Crust in Austria, Exc. Guide "Geology of the Moravian Zone". Krems, pp 14–22

de Blasio FV (2011) Introduction to the physics of landslides: lecture notes on the dynamics of mass wasting. Springer, Netherlands, Dordrecht

Demek J (1996) Failure of the Dyje River valley slopes near the village Vranov nad Dyjí: facts and hypothesis. Příroda, Sborník Prací Ochrany Přírody, Praha 3:55–62 (in Czech)

Demek, J, Kopecký J (1999) Geomorphological survey of the vicinity of caves Ledové sluje in the National Park Podyjí, Czech Republic, in: Pseudokarst Reports 1. Czech Speleological Society, Prague, pp 11–22. (in Czech)

Demek J, Kopecký J (1996) Slope failures in metamorphic basement rock of the Dyje River valley, Podyjí National Park. Czech Republic Morav Geogr Reports 4:2–11

Dikau R, Brunsden D, Schrott L, Ibsen ML (1996) Landslide recognition. Identification, Movement and Causes. Willey, Chichester

Dudek A (1980) The crystalline basement block of the Outer Carpathians in Moravia: Bruno-Vistulicum. Rozpr Československé Akad Věd 90:1–85 (in Czech)

Dunne J, Elmore D, Muzikar P (1999) Scaling factors for the rates of production of cosmogenic nuclides for geometric shielding and attenuation at depth on sloped surfaces. Geomorphology 27:3–11. https://doi.org/10.1016/S0169-555X(98)00086-5

Filek E (1895) Die Freiner Eisleiten. Mittheilungen Der Sektion Für Naturkunde Des Österreichischen Touristen-Club 7(8):57–60 (in German)

Hammerl C (2017) Historical earthquake research in Austria. Geosci Lett 4:1–13. https://doi.org/10.1186/S40562-017-0073-8/FIGURES/6

Hammerl C, Lenhardt W (2013) Erdbeben in Niederösterreich von 1000 bis 2009 n. Chr. Abh. Geol. B.-A., 67, Wien. (in German)

Hartvich F, Mentlík P (2010) Slope development reconstruction at two sites in the Bohemian Forest Mountains. Earth Surf Proc Land 35:373–389. https://doi.org/10.1002/esp.1932

He L, Coggan J, Stead D, Francioni M, Eyre M (2022) Modelling discontinuity control on the development of Hell's Mouth landslide. Landslides 19:277–295. https://doi.org/10.1007/s10346-021-01813-3

Heincke B, Günther T, Dalsegg E et al (2010) Combined three-dimensional electric and seismic tomography study on the Åknes rockslide in western Norway. J Appl Geophy 70:292–306. https://doi.org/10.1016/J.JAPPGEO.2009.12.004

Hilger P, Hermanns RL, Gosse JC, Jacobs B, Etzelmüller B, Krautblatter M (2018) Multiple rock-slope failures from Mannen in Romsdal Valley, western Norway, revealed from Quaternary geological mapping and ^{10}Be exposure dating. The Holocene 1841–1854. https://doi.org/10.1177/0959683618798165

Hilger P, Hermanns R, Czekirda J, Myhra KS, Gosse J, Etzelmüller B (2021) Permafrost as a first order control on long-term rock-slope deformation in the (Sub-) Arctic Norway. Quat Sci Rev 251. https://doi.org/10.1016/jquascirev.2020.106718

Hrádek M (1998) Introduction into the project stability relations of supporting systems and tunnels in stress fields of zones of gravitational spreading". Studia Geographica 1998:140–160

Hubatka F (2001) Použití georadaru při mapování geologické stavby pokryvných útvarů a svahových pohybů. Thayensia 4:215–218 (in Czech)

Ivan A, Kirchner K (1994) Geomorphology of the Podyjí National Park in the southeastern part of the Bohemian Massif (South Moravia). Morav Geogr Reports 2:2–25

Ivy-Ochs S, Kober F (2008) Surface exposure dating with cosmogenic nuclides. E&G Quat Sci J 57:179–209. https://doi.org/10.3285/EG.57.1-2.7

Jankovská V, Baroň I, Nývlt D, Krejčí O, Krejčí V (2018) Last glacial to Holocene vegetation succession recorded in polyphase slope-failure deposits on the Maleník Ridge, Outer Western Carpathians. Quatern Int 470:38–52. https://doi.org/10.1016/j.quaint.2017.10.048

Jarman D (2006) Large rock slope failures in the Highlands of Scotland: characterisation, causes and spatial distribution. Eng Geol 83:161–182. https://doi.org/10.1016/j.enggeo.2005.06.030

Jarman D, Harrison S (2019) Rock slope failure in the British mountains. Geomorphology 340:202–233. https://doi.org/10.1016/j.geomorph.2019.03.002

Kirchner K, Ivan A (1994) K rozšíření tvarů zvětrávání v Národním parku Podyjí (jižní Morava). Fifth International Symposium on Pseudokarst, Beskid Slaski, Szcyrk, 6 pp

Klimeš J, Rowberry MD, Blahůt J, Briestenský M, Hartvich F, Košťák B, Rybář J, Stemberk J, Štěpančíková P (2012) The monitoring of slow-moving landslides and assessment of stabilisation measures using an optical–mechanical crack gauge. Landslides 9(3):407–415. https://doi.org/10.1007/s10346-011-0306-4

Kopecký J (1996) Investigation and documentation of the pseudokarst caves "Ledové sluje" in the Podyjí National Park. Příroda, Sborník Prací Ochrany Přírody, Praha 3:7–26 (in Czech)

Korup O, Clague JJ, Hermanns RL, Hewitt K, Strom AL, Weidinger JT (2007) Giant landslides, topography, and erosion. Earth Planet Sci Lett 261:578–589. https://doi.org/10.1016/j.epsl.2007.07.025

Košťák B (2001) Rock movements of the Ledové sluje slope. Thayensia 4:227–233 (in Czech)

Koutek J (1934) O vranovských ledových slujích (Eisleiten) v Podyjí. Časopis Vlasteneckého spolku musejního v Olomouci, Olomouc, XLVII:90–91. (in Czech)

Kundzewicz ZW (2007) Summer 1997 flood in Poland in perspective. In: Vasiliev OF, van Gelder PHAJM, Plate EJ, Bolgov MV (ed) Extreme Hydrological Events: New Concepts For Security. Conf. Proc., Springer, pp 97–110

Lang A, Moya J, Corominas J, Schrott L, Dikau R (1999) Classic and new dating methods for assessing the temporal occurrence of mass movements. Geomorphology 30:33–52. https://doi.org/10.1016/S0169-555X(99)00043-4
Le Roux O, Schwartz S, Gamond JF, Jongmans D, Bourles D, Braucher R, Mahaney W, Carcaillet J, Leanni L (2009) CRE dating on the head scarp of a major landslide (Séchilienne, French Alps), age constraints on Holocene kinematics. Earth Planet Sci Lett 280:236–245. https://doi.org/10.1016/J.EPSL.2009.01.034
Lenart J (2015) Morphological patterns of crevice-type caves in sedimentary rocks of the outer Western Carpathians (Czech Republic). J Cave Karst Stud 77(3):165–176. https://doi.org/10.4311/2014ES0113
Lenhardt WA, Švancara J, Melichar P, Pazdírková J, Havíř J, Sýkorová Z (2007) Seismic activity of the Alpine-Carpathian-Bohemian Massif region with regard to geological and potential field data. Geol Carpathica 58:397–412
Lesage G, Byrne K, Morris WA et al (2019) Interpreting regional 3D fault networks from integrated geological and geophysical data sets: an example from the Guichon Creek batholith, British Columbia. J Struct Geol 119:93–106. https://doi.org/10.1016/J.JSG.2018.12.007
Loke MH, Barker RD (1996) Rapid least-squares inversion of apparent resistivity pseudosections by a quasi-Newton method. Geophys Prospect 44:131–152. https://doi.org/10.1111/j.1365-2478.1996.tb00142.x
Margielewski W, Urban J (2017) Gravitationally induced non-karst caves: tectonic and morphological constrains, classification, and dating; Polish Flysch Carpathians case study. Geomorphology 296:160–181. https://doi.org/10.1016/j.geomorph.2017.08.018
Margielewski W, Urban J (2003) Crevice-type caves as initial forms of rock landslide development in the Flysch Carpathians. Geomorphology 54:325–338. https://doi.org/10.1016/S0169-555X(02)00375-6
Meentemeyer RK, Moody A (2000) Automated mapping of conformity between topographic and geological surfaces. Comput Geosci 26:815–829. https://doi.org/10.1016/S0098-3004(00)00011-X
Merchel S, Bremser W (2004) First international 26Al interlaboratory comparison - part I. Nucl Instrum Methods Phys Res, Sect B 223–224:393–400. https://doi.org/10.1016/j.nimb.2004.04.076
Migoń P, Jancewicz K, Rózycka M, Duszyński F, Kasprzak M (2017) Large-scaleslope remodelling by landslides – geomorphic diversity and geological controls, Kamienne Mts. Central Europe Geomorphology 289:134–151. https://doi.org/10.1016/j.geomorph.2016.09.037
Milsom J, Eriksen A (2011) Field geophysics. John Wiley & Sons. https://doi.org/10.1002/9780470972311
Müller K, Polom U, Winsemann J et al (2020) Structural style and neotectonic activity along the Harz Boundary Fault, northern Germany: a multimethod approach integrating geophysics, outcrop data and numerical simulations. Int J Earth Sci 109:1811–1835. https://doi.org/10.1007/S00531-020-01874-0
Murphy B (2015) Coseismic landslides. In: Davies T (ed) Landslide hazards, risks and disasters. Elsevier, Amsterdam, pp 91–129
Nemčok A (1972) Gravitational slope deformation in high mountains. Proceedings of the 24th International Geological Congress, Montreal: Spain, vol. 13:132–141
Pánek T (2019) Landslides and Quaternary climate changes: the state of the art. Earth-Sci Rev 196:102871. https://doi.org/10.1016/j.earscirev.2019.05.015
Pánek T, Engel Z, Mentlík P, Braucher R, Břežný M, Škarpich V, Zondervan A (2016) Cosmogenic age constraints on post-LGM catastrophic rock slope failures in the Tatra Mountains (Western Carpathians). CATENA 138:52–67. https://doi.org/10.1016/j.catena.2015.11.005
Pánek T, Hartvich F, Jankovská V, Klimeš J, Tábořík P, Bubík M, Smolková V, Hradecký J (2014) Large Late Pleistocene landslides from the marginal slope of the Flysch Carpathians. Landslides 11:981–992. https://doi.org/10.1007/s10346-013-0463-8
Pánek T, Margielewski W, Tábořík P, Urban J, Hradecký J, Szura C (2010) Gravitationally induced caves and other discontinuities detected by 2D electrical resistivity tomography: case studies from the Polish Flysch Carpathians. Geomorphology 123:165–180. https://doi.org/10.1016/j.geomorph.2010.07.008
Pánek T, Mentlík P, Engel Z, Braucher R, Zondervan A, Aster Team (2017) Late Quaternary sackungen in the highest mountains of the Carpathians. Quatern Sci Rev 159:47–62. https://doi.org/10.1016/j.quascirev.2017.01.008
Place J, Géraud Y, Diraison M et al (2016) Structural control of weathering processes within exhumed granitoids: compartmentalisation of geophysical properties by faults and fractures. J Struct Geol 84:102–119. https://doi.org/10.1016/J.JSG.2015.11.011
Počta J, Schönbeková M (1991) Ledové sluje. CHKO Podyjí. Special Map 1 : 200. ČÚOP, Praha
Pospíšil L, Pazdírek O (1998) "Ice Grottos" - test geophysical survey. Thayensia 1:53–58 (in Czech)
Pospíšil L, Pazdírek O, Frolka J et al (1997) Analýza strukturně tektonických poměrů území NP Podyjí se zvláštním zřetelem na lokalitu "Ledové sluje". Archiv Národní park Podyjí, p. 15 (in Czech)
Raška P, Zábranský V, Brázdil R, Lamková J (2016) The late Little Ice Age landslide calamity in North Bohemia: triggers, impacts and post-landslide development reconstructed from documentary data (case study of the Kozí vrch Hill landslide). Geomorphology 255:95–107. https://doi.org/10.1016/j.geomorph.2015.12.009
Riva F, Agliardi F, Amitrano D, Crosta GB (2018) Damage-based time-dependent modeling of paraglacial to postglacial progressive failure of large rock slopes. JGR-Earth Surface 123:124–141. https://doi.org/10.1002/2017JF004423
Roštínský P, Pospíšil L, Švábenský O (2013) Recent geodynamic and geomorphological analyses of the Diendorf-Čebín Tectonic Zone, Czech Republic. Tectonophysics 599:45–66. https://doi.org/10.1016/j.tecto.2013.04.008
Schramm JM, Weidinger JT, Ibetsberger HJ (1998) Petrologic and structural controls on geomorphology of prehistoric Tsergo Ri slope failure, Langtang Himal. Nepal Geomorphology 26:107–121. https://doi.org/10.1016/S0169-555X(98)00053-1
Schulmann K, Melka R, Lobkowicz MZ, Ledru P, Lardeaux JM, Autran A (1994) Contrasting styles of deformation during progressive nappe stacking at the southeastern margin of the Bohemian Massif (Thaya Dome). J Struct Geol 16:355–370. https://doi.org/10.1016/0191-8141(94)90040-X
Schwartz S, Zerathe S, Jongmans D, Baillet L, Carcaillet J, Audin L, Dumont T, Bourlès D, Braucher R, Lebrouc V (2017) Cosmic ray exposure dating on the large landslide of Séchilienne (Western Alps): a synthesis to constrain slope evolution. Geomorphology 278:329–344. https://doi.org/10.1016/J.GEOMORPH.2016.11.014
Špaček P (2021) Diendorf-Boskovice fault system. In: Špaček P, Štěpančíková P, Prachař I (eds) Faults of the Bohemian Massif – source of analytical data on main faults and faulted areas with seismogenic potential. IPE, Masaryk University. https://doi.org/10.48790/MWF4-SH44
Špaček P, Bábek O, Štěpančíková P, Švancara J, Pazdírková J, Sedláček J (2015) The Nysa-Morava Zone: an active tectonic domain with Late Cenozoic sedimentary grabens in the Western Carpathians' foreland (NE Bohemian Massif). Int J Earth Sci 104:963–990. https://doi.org/10.1007/s00531-014-1121-7
Špaček P, Valenta J, Tábořík P, Ambrož V, Urban M, Štěpančíková P (2017) Fault slip versus slope deformations: experience from paleoseismic trenches in the region with low slip-rate faults and strong Pleistocene periglacial mass wasting (Bohemian Massif). Quat Int 451:56–73. https://doi.org/10.1016/J.QUAINT.2017.05.006
Špalek V (1935) Ledové sluje u Vranova nad Dyjí. Sborník ČSZ 41:49–55 (in Czech)
Starkel L, Michczyńska D, Krąpiec M, Margielewski W, Nalepka D, Pazdur A (2013) Progress in the Holocene chrono-climatostratigraphy of Polish territory. Geochronometria 40:1–21. https://doi.org/10.2478/s13386-012-0024-2
Stead D, Eberhardt E (2013) Understanding the mechanics of large landslides. Ital J Eng Geol Environ 6:85–112. https://doi.org/10.4408/IJEGE.2013-06.B-07
Stone JO (2000) Air pressure and cosmogenic isotope production. Journal of Geophysical Research: Solid Earth 105:23753–23759. https://doi.org/10.1029/2000JB900181
Strauhal T, Zangerl C, Fellin W, Holzmann M, Engl DA, Brandner R, Tropper P, Tessadri R (2017) Structure, mineralogy and geomechanical properties of shear zones of deep-seated rockslides in metamorphic rocks (Tyrol, Austria). Rock Mech Rock Eng 50(2):419–438. https://doi.org/10.1007/s00603-016-1113-y
Suess FE (1912) Die Moravischen Fenster und ihre Beziehung zum Grundgebirge des Hohen Gesenke. Denkrsch. K. Akad. Wiss., Math. Naturwiss. (in German)

Táborík P, Lenart J, Blecha V, Vilhelm J, Turský O (2017) Geophysical anatomy of counter-slope scarps in sedimentary flysch rocks (Outer Western Carpathians). Geomorphology 276:59–70. https://doi.org/10.1016/j.geomorph.2016.09.038

Wagner J (2001) The research and documentation of the pseudokarst caves in the Podyjí National Park until 2001. Thayensia 4:263–266 (in Czech)

Weidinger JT, Korup O (2009) Frictionite as evidence for a large Late Quaternary rockslide near Kanchenjunga, Sikkim Himalayas, India – implications for extreme events in mountain relief destruction. Geomorphology 103:57–65. https://doi.org/10.1016/j.geomorph.2007.10.021

Zangerl C, Eberhardt E, Perzlmaier S (2010) Kinematic behaviour and velocity characteristics of a complex deep-seated crystalline rockslide system in relation to its interaction with a dam reservoir. Eng Geol 112:53–67. https://doi.org/10.1016/j.enggeo.2010.01.001

Zerathe S, Lebourg T, Braucher R, Bourlès D (2014) Mid-Holocene cluster of large-scale landslides revealed in the Southwestern Alps by 36Cl dating. Insight on an Alpine-scale landslide activity. Quat Sci Rev 90:106–127. https://doi.org/10.1016/J.QUASCIREV.2014.02.015

Zvelebil J, Košťák B, Novotný J, Andrejkovič T (1997) Extensive failure of a low slope in massive orthogneiss. Engineering geology and the environment. Proc. symposium, Athens, 1997, 1:1159–1165

Zvelebil J, Novotný J, Košťák B, Zika P (1996) Preliminary results of engineering-geological study of slope deformation of Ledové sluje crest. Příroda, Sborník Prací Ochrany Přírody, Praha 3:41–54 (in Czech)

Jan Lenart (✉) · **Tomáš Pánek**
Department of Physical Geography and Geoecology, Faculty of Science, University of Ostrava, Chittussiho 10, 710 00 Ostrava, Czechia
Email: jan.lenart@osu.cz

Martin Kašing
Department of Geological Engineering, Faculty of Mining and Geology, VSB – Technical University of Ostrava, 17. listopadu 15, 708 00, Ostrava, Czechia

Régis Braucher
Aix-Marseille Université, CEREGE, CNRS, Collège de France, INRAE, UM 34, 13545 Aix-en-Provence, France

František Kuda
Department of Environmental Geography, Institute of Geonics, Czech Academy of Sciences, Drobného 28, 602 00 Brno, Czechia